THE JOURNAL OF BIOLOGICAL CHEMISTRY
Vol. 279, No. 10, Issue of March 5, pp. 9176–9189, 2004

Printed in U.S.A.

Properties of Some Variants of Human β_2-Microglobulin and Amyloidogenesis*[S]

Received for publication, September 30, 2003, and in revised form, December 2, 2003
Published, JBC Papers in Press, December 4, 2003, DOI 10.1074/jbc.M310779200

Alessandra Corazza‡, Fabio Pettirossi‡, Paolo Viglino‡, Giuliana Verdone‡, Julian Garcia§, Pascal Dumy§, Sofia Giorgetti¶, Palma Mangione¶‖, Sara Raimondi¶‖, Monica Stoppini¶, Vittorio Bellotti¶‖, and Gennaro Esposito‡

From the ‡Dipartimento di Scienze e Tecnologie Biomediche and Microgravity, Aging, Training, and Immobility, Centre of Excellence, Università di Udine, Piazzale Kolbe 4, 33100 Udine, Italy, §Laboratoire d'Etudes Dynamiques et Structurales de la Sélectivité, University Joseph Fourier of Grenoble, 38041 Grenoble Cedex 9, France, the ¶Dipartimento di Biochimica via Taramelli 3/b Università di Pavia, 27100 Pavia, Italy, and the ‖Laboratorio di Biotecnologie Istituto di Recovero e Cura a Carattere Scientifico, Policlinico S. Matteo, 27100 Pavia, Italy

Three variants of human β_2-microglobulin (β_2-m) were compared with wild-type protein. For two variants, namely the mutant R3Aβ_2-m and the form devoid of the N-terminal tripeptide (ΔN3β_2-m), a reduced unfolding free energy was measured compared with wild-type β_2-m, whereas an increased stability was observed for the mutant H31Yβ_2-m. The solution structure could be determined by ^{1}H NMR spectroscopy and restrained modeling only for R3Aβ_2-m that showed the same conformation as the parent species, except for deviations at the interstrand loops. Analogous conclusions were reached for H31Yβ_2-m and ΔN3β_2-m. Precipitation and unfolding were observed over time periods shorter than 4–6 weeks with all the variants and, sometimes, with wild-type protein. The rate of structured protein loss from solution as a result of precipitation and unfolding always showed pseudo-zeroth order kinetics. This and the failure to observe an unfolded species without precipitation suggest that a nucleated conformational conversion scheme should apply for β_2-m fibrillogenesis. The mechanism is consistent with the previous and present results on β_2-m amyloid transition, provided a nucleated oligomeric species be considered the stable intermediate of fibrillogenesis, the monomeric intermediate being the necessary transition step along the pathway from the native protein to the nucleated oligomer.

Over the last several years, an overwhelming number of reports have addressed the phenomenon of amyloidogenesis. The interest in the subject stems not only from the social relevance of amyloid pathologies such as Alzheimer's disease, or spongiform encephalopathy, or the various systemic amyloidoses, but also from the general implications in the issue of protein folding.

Amyloidoses have been recognized as conformational diseases that arise from the conversion of globular proteins into insoluble fibrillar aggregates (1). Despite the diversity of the involved proteins, amyloid fibrils exhibit a common structure known as cross-β structure, which appears to be a particularly stable, generic protein fold, accessible to many polypeptide chains under specific conditions *in vitro* and *in vivo* (2). The amyloid deposition of β_2-microglobulin (β_2-m),[1] the nonpolymorphic light chain of the class I major histocompatibility complex (MHC-I), is associated to dialysis-related amyloidosis (3). The disease is the result of long term hemodialysis in individuals with chronic renal failure, a widespread pathology with high social costs that are further increased by the inevitable dialysis-related amyloidosis complication. Recently ankylosing spondylitis has also been proposed to originate from β_2-m deposition (4). We determined the solution structure of isolated β_2-m by NMR spectroscopy (5) and showed that the most important rearrangements of the protein, with respect to its structure in MHC-I, were observed for strands D and E, interstrand loop D-E, and strand A, including the N-terminal segment. We stated that these modifications can be considered as the prodromes of the amyloid transition that starts at sheet 1 with the rupture of strand A pairing, and leads to polymerization, through intermolecular pairing at strand D and probably strand C, and precipitation into fibrils, *i.e.* according to the scheme we had proposed earlier from a comparative investigation on the full-length protein and the form devoid of the six N-terminal residues (ΔN6β_2-m) (6). This latter species, which accounts for ~30% of β_2-m content in *ex vivo* fibrils, had been shown to possess a higher tendency to self-aggregate than the full-length protein and to fail reaching a fully folded native state at the end of the refolding procedure (7). Successive works reporting ^{1}H-^{15}N NMR studies of pH and urea-driven denaturation experiments (8) and deuterium exchange of backbone amides (9) confirmed the amyloid pairing pattern of β_2-m that was inferred from our former results (6). Moreover, in analogy with the solution structure, even the crystal structure of isolated human β_2-m has been claimed to reveal the clues to its amyloidogenic properties (10). However, the *revelations* that

* This work was supported by grants from the Italian Ministry of Education (Fondo per gli Investimenti della Ricerca di Base, Cofin), the Italian Ministry of Health (Progetto Finalizzato Alzheimer 2000), and the Dipartimento di Scienze e Tecnologie Biomediche - University of Udine. The costs of publication of this article were defrayed in part by the payment of page charges. This article must therefore be hereby marked "*advertisement*" in accordance with 18 U.S.C. Section 1734 solely to indicate this fact.

[S] The on-line version of this article (available at http://www.jbc.org) contains Figures S1 and S2.

** To whom correspondence should be addressed: Dipartimento di Scienze e Tecnologie Biomediche, Università di Udine, P. le Kolbe 4, 33100 Udine, Italy. Tel.: 39-0432-494321/5; Fax: 39-0432-494301; E-mail: gesposito@mail.dstb.uniud.it.

[1] The abbreviations used are: β_2-m, β_2-microglobulin; ΔN3β_2-m, β_2-microglobulin 4–99 fragment; ΔN6β_2-m, β_2-microglobulin 7–99 fragment; GdmCl, guanidinium chloride; MD, molecular dynamics; MHC-I, class I major histocompatibility complex; NCC, nucleated conformational conversion; NOESY, nuclear Overhauser spectroscopy; ppm, parts per million; r.m.s.d., root mean square deviation; TOCSY, total correlation spectroscopy; UHBD, University of Houston Brownian Dynamics; HLA, human leukocyte antigen.

are disclosed by the crystal structure appear quite different from the elements of the solution structure that were recognized to forerun the amyloid transformation of β_2-m and hence considered as prodromes of the process (5). To confirm and reinforce our model, we present here the results of the characterization by classical biochemical methods and ^{1}H NMR of three variants of human β_2-m, namely the truncated form ΔN3β_2-m and the mutants R3Aβ_2-m and H31Yβ_2-m. These species were designed to test the role of some structural elements affecting the stability of the isolated wild-type protein in solution (5, 6). The truncated form corresponds to the wild-type protein devoid of the three N-terminal residues. In the mutants, the wild-type sequence residues in position 3 and 31, *i.e.* an arginyl and a histidyl residue, respectively, are replaced with an alanyl and a tyrosyl residue, respectively.

EXPERIMENTAL PROCEDURES

Preparation of Recombinant Protein Samples—Expression and purification of recombinant proteins was carried out as previously reported for β_2-m and ΔN6β_2-m (6). cDNA corresponding to the truncated species of β_2-m lacking the first three (ΔN3β_2-m) residues was accomplished by PCR amplification of the full length cDNA with the primers 5′-CGCACATATGACTCCAAAGATTCAGG and 3′-GCCGGATCCTTACATGTCTCGATCCCAC. Mutagenesis of His-31 into Tyr and Ser, and of Arg-3 into Ala were performed by using the QuikChange™ site-directed mutagenesis kit supplied by Stratagene (La Jolla, CA). The following primers were used: for H31Y, 5′-GCTATGTGTCTGGGTTTTATCCATCCGACATTGAAG and 3′-CTTCAATGTCGGATGGATAAAACCCAGACACATAGC; for H31S, 5′-GCTATGTGTCTGGGTTTTCTCCATCCGACATTGAAG and 3′-CTTCAATGTCGGATGGAGAAAACCCAGACACATAGC; for R3A, 5′-CGCACATATGATCCAGGCTACTCCAAAGATTCAGG and 3′-CCTTGAATCTTTGGAGTAGCCTGGATCATATGTGCG.

The constructs were always introduced in the same BL21 *Escherichia coli* strain. A methionine residue was present at the N-terminal position of all recombinant products that will be referred to as Met-0. All the recombinant proteins gave a single species when assayed by electrospray-ionization mass spectrometry performed with ~20 μM samples. The concentration of the protein samples was determined spectrophotometrically at 280 nm: $A^{1\,cm}_{1\%}$ = 16.17 (β_2-m), 16.29 (R3Aβ_2-m), 16.24 (H31Sβ_2-m), 17.21 (H31Yβ_2-m), 16.73 (ΔN3β_2-m), and 17.22 (ΔN6β_2-m).

Determination of Folding Stability—The thermodynamic stability was determined by monitoring the dependence of intrinsic tryptophan fluorescence on guanidinium chloride (GdmCl) concentration. Excitation was at 295 nm and emission monitored in the range 300–500 nm (11) using slit widths of 5 nm. The protein concentration of all samples was 25 μg ml^{-1} in 20 mM sodium phosphate buffer, pH 7.3, with GdmCl concentrations ranging from 0 to 4 M. The protein/denaturant solutions were pre-equilibrated at 293 K for 20 min. Fluorescence spectra were obtained with a PerkinElmer LS50B spectrofluorimeter (PerkinElmer Life Sciences).

Experimental data were converted to the unfolded fraction using $f_U = (y - y_N)/(y_U - y_N)$, where y is the value of the spectroscopic parameter observed at a given denaturant concentration, and y_N and y_U are the values of the native and unfolded protein, respectively, extrapolated from the pre- and post-transition base lines defined by a nonlinear least square fitting procedure (12). The free energy of unfolding in the absence of the denaturant, $\Delta G°(H_2O)$, and the denaturant concentration at the midpoint of the unfolding transition, C_m, were calculated according to the linear extrapolation model (13) assuming a two-state transition.

Kinetics Determinations—Folding and unfolding kinetics were monitored for β2m-wild type and mutants on a Bio-Logic SFM-300 stopped flow fluorimeter, by using an excitation wavelength of 295 nm and monitoring the total fluorescence emission change at 320 nm (14, 15). All the experiments were performed at 303 K in 10 mM sodium phosphate buffer, pH 7.4, at a 0.02 mg ml^{-1} final protein concentration. The unfolding reactions were performed by a 10-fold dilution of a denaturant-free solution of each protein at 0.2 mg ml^{-1} with solutions containing various concentrations of GdmCl to obtain a final GdmCl molarity ranging from 2 to 5.4 M. The refolding experiments were performed by a 25-fold dilution of protein samples at 0.5 mg ml^{-1}, unfolded in 4 M GdmCl, into final solutions containing denaturant concentrations from 0 to 1 M. Slow changes of fluorescence during folding were followed at 303 K by a PerkinElmer LS50B fluorimeter using excitation and emission wavelengths of 295 and 340 nm, respectively, with a 10-mm path-length cell. For each protein, one volume of 0.2 mg ml^{-1} solution, denatured at equilibrium in 4 M GdmCl, was mixed with nine volumes of 10 mM sodium phosphate, pH 7.4. All the kinetic traces were fitted as previously described (14, 15).

NMR Spectroscopy—NMR spectra were obtained at 500.13 MHz with a Bruker Avance spectrometer on 0.4–0.9 mM protein samples dissolved in H_2O/D_2O 90/10 and 95/5 or 99.9% D_2O with 50–70 mM phosphate buffer, 50–100 mM NaCl, and pH* in the range 6.2–6.7 (pH* is the pH meter reading without isotope effect correction). When necessary, samples were centrifuged and/or filtered using filters with a threshold of 0.22 μm (Millipore, Bedford, MA). The studies were carried out at 310 K, with only a few experiments obtained at 298, 303, or 307 K with H31Yβ_2-m for assignment controls. A number of two-dimensional TOCSY (16), double quantum-filtered correlation spectroscopy (17) and NOESY (18) spectra were acquired. The adopted experimental schemes included solvent suppression by presaturation, or WATERGATE (19) and excitation sculpting (20), 1–1.5-s steady state recovery time, mixing times (t_m) of 13–50 ms for TOCSY and 50–150 ms for NOESY, t_1 quadrature detection by time proportional phase incrementation (21), or States method (22), or gradient-assisted coherence selection (echo-antiecho) (23). The spin-lock mixing of the TOCSY experiment was obtained with MLEV17 (24) or DIPSI-2 (25) pulse trains at $\gamma B_2/2\pi$ = 7–10 kHz. The acquisitions were performed over a spectral width of 7002.801 Hz in both dimensions (or, sometimes, 8012.820 Hz), with matrix size of 1024–2048 points in t_2 and 256–600 points in t_1, and 32–128 scans each t_1 FID. For the observation of very rapidly relaxing spin systems, the acquisition time was reduced in both dimensions by collecting data matrices of smaller size (512–1024 points in t_2 and 128–256 points in t_1). Precipitation was followed by collecting series of one-dimensional spectra, and sometimes also two-dimensional TOCSY, at regular time intervals over periods of 7–20 days. Acquisition conditions for two-dimensional data were the same as above reported, whereas for one-dimensional data time domains were set at 4096–8192 points, with relaxation delays of 1.1 or 10 s, depending on whether a steady or an equilibrium state integral was needed. Refolding of the wild-type protein was also followed by one-dimensional NMR measurements. After incubating at ambient temperature, for approximately 1 h, 1 mg of protein in 100 μl of 3.0 M GdmCl in D_2O, the solution was transferred into the NMR tube and diluted 20-fold with the renaturing buffer (70 mM phosphate, 100 mM NaCl, in D_2O, pH* = 7.5). The sample was then put into the magnet and, after quick equilibration and spectrometer adjustments, one-dimensional spectra were collected at regular intervals (1.5 min), at 298 K, using excitation sculpting (20) to suppress the residual HOD peak, 2048 time-domain data points, 64 scans/experiment, and 8 dummy scans. The first acquisition was completed at 6.5 min from dilution, and, overall, the refolding kinetics was monitored by this real-time NMR approach for approximately 90 min. The achievement of a steady state was checked by recording spectra at higher intervals (>24 h) on the sample left in the magnet at the same initial conditions. Data processing and analysis were performed using Felix (Accelrys Inc., San Diego, CA) software with shifted (60–90°) square sinebell apodization, zero filling (up to 2048 × 2048 real points) and polynomial base-line correction for NOESY data. All ΔN3β_2-m and R3Aβ_2-m spectra were referenced on the Leu-23 $C^\delta H_3$ resonance at −0.58 ppm as previously reported (6). For H31Yβ_2-m spectra were referenced using the Leu-23 $C^\delta H_3$ resonance peak (−0.566 ppm at 310 K), whose chemical shift was determined at varying temperature with respect to internal dioxane (always at 3.750 ppm). Internuclear distances were quantified only for R3Aβ_2-m from the NOESY cross-peak volumes of Trp-95, as previously reported (5). Tethered molecular dynamics (MD) simulations were performed by using the Discover software (Accelrys Inc., San Diego, CA) and following the default protocol for simulated annealing (8.6-ps MD, 500 conjugate-gradient minimization steps) (26). Molecular structures were generated with InsightII (Accelrys Inc., San Diego, CA), MOLMOL (27), and Swiss-PdbViewer (www.expasy.ch/spdbv/mainpage.html).

pK_a and Free Energy Calculations—The electrostatic contributions to free energy were computed with the UHBD (University of Houston Brownian Dynamics) program, which is capable of solving the linearized Poisson-Boltzmann equation using a finite-difference method (28) in a continuum solvent model. The pK_a values for the ionizable residues of the protein and the related electrostatic free energy contributions (ΔG_{el}) were calculated according the methodology of Antosiewicz (29–30). The solvation contribution to the free energy of protein folding (ΔG_{sol}) was calculated according to Eisenberg *et al.* (31) with a routine implemented in the program Tinker (J. W. Ponder, Washington University School of Medicine, Saint Louis, MO). The method is semiempirical and calculates, for every atom i, the free energy of transfer, ΔG_i,

TABLE I
Themodynamic stability parameters obtained for wild-type β_2-m and variants

b_2-m variant	C_m[a][GdmCl]	$\Delta G°(H_2O)$[b]
		kcal mol^{-1}
Wild-type β_2-m	2.3	6.3 ± 0.2
H31Yβ_2-m	2.9	7.8 ± 0.4
H31Sβ_2-m	2.5	6.9 ± 0.3
R3Aβ_2-m	2.2	5.9 ± 0.2
ΔN3β_2-m	1.9	4.4 ± 0.2
ΔN6β_2-m	1.65	3.78 ± 0.09

[a] Column shows denaturant concentration at the midpoint of the unfolding transition.
[b] Column shows free energy of unfolding in the absence of denaturant at 293 K and pH = 7.3.

from the environment of the protein interior to solution, according to $\Delta G_i = \Delta\sigma_i A_i$, where $\Delta\sigma_i$ is the atomic solvation parameter (31) and A_i is the accessible surface area of the atom. The total ΔG_{sol} for the protein is obtained by summing over all protein atoms.

RESULTS

GdmCl Denaturation—The denaturation of wild-type and variant β_2-m species was measured from the changes in fluorescence upon addition of GdmCl, and the results are presented in Table I and Fig. 1. ΔN6β_2-m appears to be the least stable species followed by ΔN3β_2-m and R3Aβ_2-m, which show intermediate $\Delta G°$ and C_m values between wild type and ΔN6β_2-m. The alanyl substitution for arginyl in position 3 destabilizes the molecule by 0.4 kcal mol^{-1}, whereas the truncation at the same location destabilizes by 1.9 kcal mol^{-1}. On the other hand, the presence of a tyrosyl residue in position 31 stabilizes β_2-m by 1.5 kcal mol^{-1}, in qualitative agreement with the result obtained for the β_2-m His-31 → Phe mutant (2.6 kcal mol^{-1} stabilization under different conditions (Ref. 32)), whereas the introduction of a serine in the same position results in a reduced stabilization (6.9 kcal mol^{-1}).

Unfolding/Refolding Kinetics—In wild-type β_2-m, the refolding pathway is characterized by three phases, the slowest of which has a rate constant of 0.0032 ± 0.0005 s^{-1} (14). This slow refolding phase of β_2-m was also investigated by real-time NMR. The spectra collected within the first 30 min from dilution with phosphate buffer of the GdmCl solution exhibited progressive changes toward the typical resonance pattern of the folded protein. A few resolved peaks appear to evolve in the upfield and aromatic regions (Fig. 2). In particular, the Ile-35 δ-methyl signal and the upfield-shifted H^β resonance of Leu-23 slowly grow up to the final intensity, whereas the γ-methyls of Val-37 seem to increase at the expense of another pair of signals that, most likely, arise from the methyls of the same residue in a different geometry within a transient conformer of the molecule. Simultaneous changes observed in the aromatic region involve the ring resonances of Tyr-66, Phe-30 and Phe-70, and Trp-95, *i.e.* the aromatic groups that are largely responsible for the upfield shifts of Val-37, Ile-35, and Leu-23, respectively. Overall, the NMR pattern suggests that a rearrangement of the hydrophobic core takes place throughout the slow refolding phase of β_2-m, consistently with the corresponding increase of 8-anilino-1-naphthalene sulfonic acid binding and changes in fluorescence and circular dichroism pattern, previously observed during the same refolding phase (14). Based on the NMR data, the rearrangement process involves a transient conformer that slowly converts into the stable, native form of the protein, with no evidence in favor of an equilibrium between the two species (15). The persistence of some 14 ± 8% of total protein in the refolding intermediate conformation (I_2) (15) could not be confirmed, although the occurrence of smaller amounts of the same species, *i.e.* below 2–3%, cannot be ruled out in principle because such small quantities would be hardly detectable by NMR. Likewise, we cannot exclude possible equilibria involving spectroscopically silent species (14), which for NMR would be either species with unresolved signals buried under the main envelope, or large aggregates with very broad linewidths, in any case other than the slowly converting form observed during refolding.

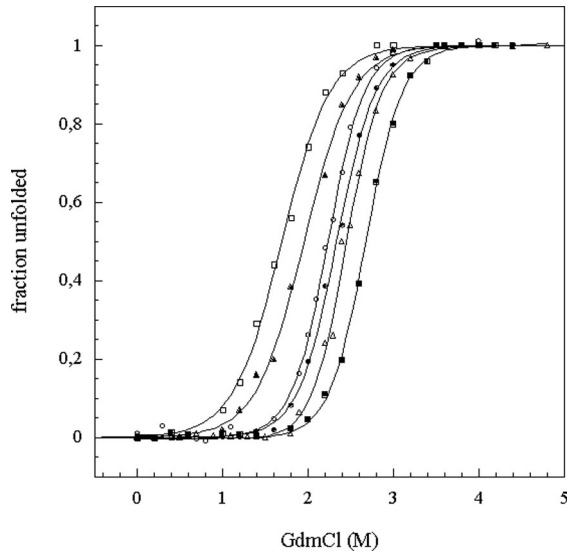

FIG. 1. **GdmCl denaturation profiles of wild-type β_2-m (●) and variants H31Yβ_2-m (■), H31Sβ_2-m (△), R3Aβ_2-m (○), ΔN3β_2-m (▲), and ΔN6β_2-m (□).** All the measurements were performed at pH 7.3 and 293 K.

As for the mutants, the increased folding stability of H31Yβ_2-m and H31Sβ_2-m prompted us to investigate the effect of the mutation on unfolding/refolding kinetics. Although the H31Yβ_2-m very fast and fast folding kinetics phases are comparable with those of wild-type β_2-m, a remarkable difference was appreciated for the slow phase that displays a rate constant of 0.031 s^{-1} for H31Yβ_2-m (Fig. 3), *i.e.* 10 times faster than the value reported for the wild-type species (14). Preliminary results show that the slow folding phase of the H31S mutant exhibits a rate constant of 0.0043 ± 0.0006 very close to that of the wild type protein. A lower unfolding rate constant for H31Yβ_2-m (6.9 ± 1.2 × 10^{-5} s^{-1}) with respect to the wild-type protein (4.9 ± 1.8 10^{-4} s^{-1}) is in perfect agreement with the increased stability of the mutant at equilibrium.

NMR Characterization—The detailed interpretation of the ^{1}H NMR spectra of the mutants and fragments of β_2-m, based on the parent spectrum of the wild-type species, is far from being trivial. As already observed with ΔN6β_2-m (6), the task requires checking and redetermining most of the resonance assignments of the variant under investigation according to the standard methodology, *i.e.* going through scalar and dipolar connectivity pattern for each amino acid residue (33). This work was performed entirely for the truncated fragment ΔN3β_2-m and the two mutants R3Aβ_2-m and H31Yβ_2-m. The corresponding assignment lists are available at the BioMagRes data bank (entry points 5782, 5783, and 5784). The relevant differences of H^α chemical shifts ($\Delta\delta H^\alpha$) with respect to the corresponding values of wild-type protein are shown in Fig. 4. For the sake of comparison, the ΔN3β_2-m and R3Aβ_2-m data (Fig. 4*A*) are not plotted in the same panel as those of H31Yβ_2-m (Fig. 4*B*) because of the gaps in the assignment list of the latter mutant. The backbone resonances within fragments 29–34, 57–58, and 60–62 of H31Yβ_2-m could not be observed in the NMR spectrum (either totally or partially for residues 58 and 62) because of exchange broadening. For the other two variants instead, the missing resonances (as a matter

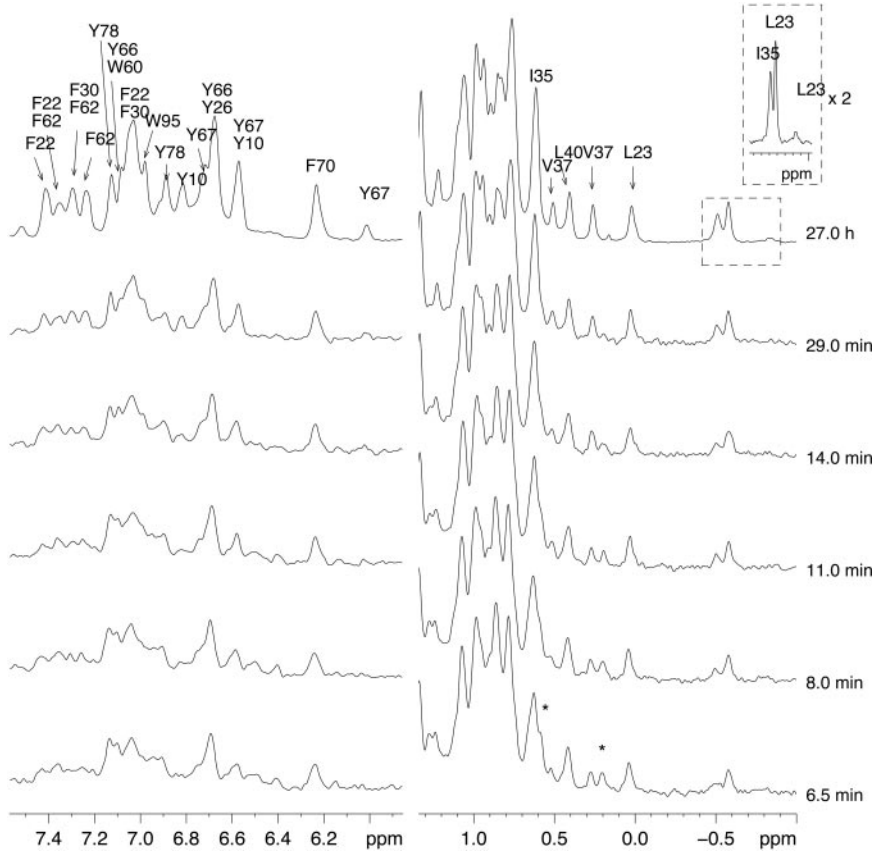

FIG. 2. **Real-time NMR monitoring of the slow folding phase of wild-type β_2-m, initially incubated in 3.0 M GdmCl and subsequently diluted with phosphate buffer.** Measurements were performed at 298 K and pH* 7.5. The δ-methyl signal of Ile-35 and the upfield-shifted H^{β} resonance of Leu-23 slowly grow up to the final intensity, whereas the γ-methyls of Val-37 seem to increase at the expense of the pair of signals that are starred in the bottom trace. Most likely, these latter resonances arise from the methyls of the same Val-37 residue in a different geometry within a transient conformer of the molecule. Obviously, a similar pattern of resonance loss and gain must occur also for the mentioned Ile-35 and Leu-23 signals, but only the gain is clearly observed as a result of spectral overlap. Simultaneously, changes are observed also in the aromatic region involving the ring resonances of Tyr-66, Phe-30 and Phe-70, and Trp-95, *i.e.* the aromatic groups that are largely responsible for the upfield shifts of Val-37, Ile-35, and Leu-23, respectively.

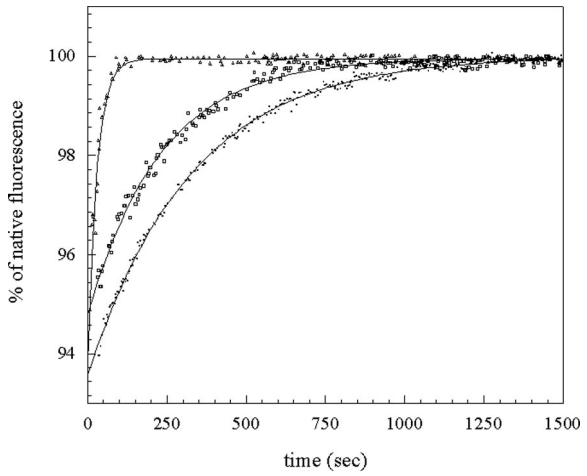

FIG. 3. **Change of intrinsic fluorescence of H31Yβ_2-m (△), H31Sβ_2-m (□), and wild type β_2-m (●) during the slow folding phase.** The kinetic traces were acquired at pH 7.4 and 303 K in the presence of 0.4 M GdmCl. The data were normalized by attributing 100% fluorescence to the native protein and fitted to a single exponential function.

of fact only a few H^N peaks) were sparsely distributed along the sequence and the trends of their $\Delta\delta H^{\alpha}$ appeared similar. Indeed, Fig. 4*A* shows that the deviations from wild-type H^{α} shifts occur essentially in the N-terminal region (residues 2–8), in the loop between strands B and C (residues 29–31), in the loop between strands D and E (residues 56–64), and in the loop between strands F and G (residues 85 and 86) for either $\Delta N3\beta_2$-m and $R3A\beta_2$-m.

However, the deviations are remarkably larger in the loop region between strands D and E and particularly for Trp-60. Similar results were obtained also for the H^N chemical shift deviations of the same molecules (data not shown). The overall deviation extent appears significantly reduced with the corresponding data of H31Yβ_2-m (Fig. 4B), *i.e.* less than ±0.05 ppm for most of the resonances, but larger differences could conceivably occur in fragments 29–34 (loop B-C) and 57–62 (loop D-E), which were not detected. The failure to observe most of the backbone resonances in these segments was ascribed to chemical exchange. Difficult detectability of some NMR signals in the same regions had been experienced with $\Delta N3\beta_2$-m and $R3A\beta_2$-m and, previously, also with wild-type β_2-m, in particular for a few residues of the interstrand loops B-C and D-E. For this latter loop, the problems arose from a conformational equilibrium leading to exchange broadening of the backbone resonances in segment 56–62, as first recognized by Okon and colleagues (34). In the interstrand loop B-C, instead, the resonances of Pro-32, which adopts a cis peptide bond geometry also in solution, were hardly observable probably as a result of the critical density of the local dipolar network, in the absence of any evidence in favor of an additional, local exchange process. Under proper conditions, the adverse consequences on the detection sensitivity of either exchange and dipolar broadening could be overcome with wild-type β_2-m, as well as for $\Delta N3\beta_2$-m and $R3A\beta_2$-m (except for a few H^N resonances). Analogous experimental conditions, however, failed to restore detectability with H31Yβ_2-m, leaving unassigned the B-C and D-E loop segments. As a matter of fact, the latter regions and the previously mentioned N-terminal and F-G loop fragments are all spatially positioned at one edge of the β_2-m molecule and therefore relatively close in space. Therefore, besides the dipolar crowding effects, the broadening that hinders observation of some backbone resonances in loop B-C could be the additional result of the exchange occurring at the adjacent D-E loop. The question arises as to why the exchange rate should be so unfavorable as to bleach out several backbone resonances in H31Yβ_2-m, contrary to wild-type protein and the other studied variants. Such an effect could be related to the increased fold

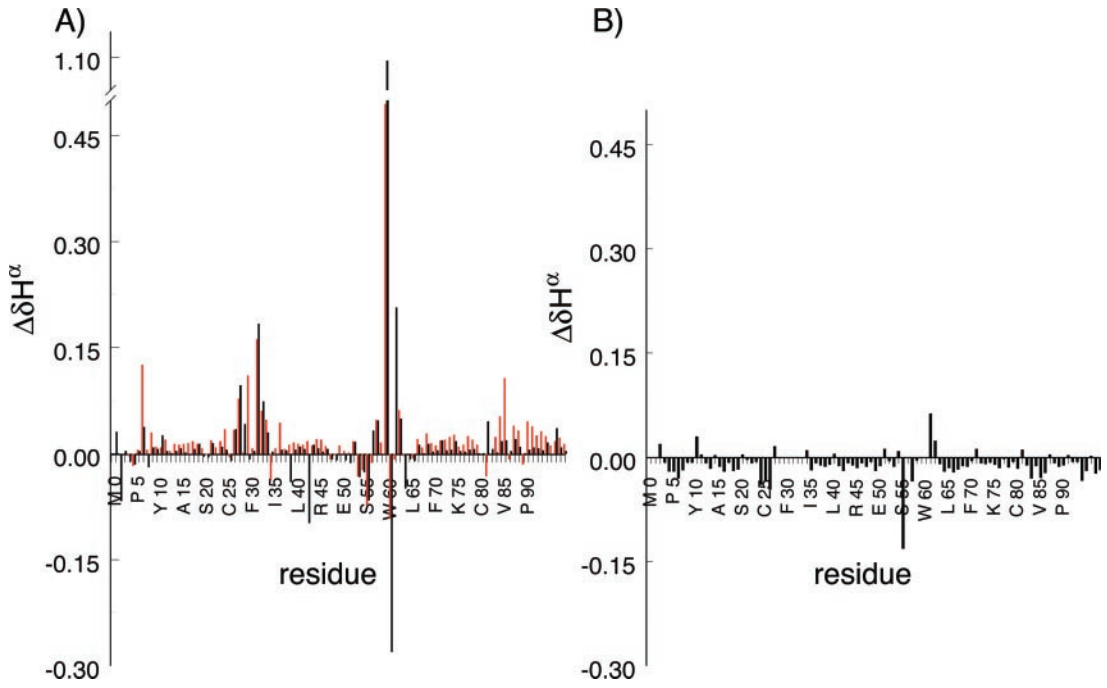

FIG. 4. **The assigned backbone H^{α} chemical shifts of the three investigated β_2-m variants are compared with the corresponding values of wild-type species obtained under similar conditions as those adopted in the present study (5).** The $\Delta\delta H^{\alpha}$ values (ppm) of R3Aβ_2-m (*A*, *black bars*), ΔN3β_2-m (*A*, *red bars*), and H31Yβ2-m (*B*) are reported as ($\delta_{variant} - \delta_{wt}$).

stability of H31Yβ_2-m, resulting in unfavorably slow conformational dynamics of the D-E loop for NMR detection. Besides the missing resonances in H31Yβ_2-m, the same area exhibits also the largest $\Delta\delta H^{\alpha}$ values measured for the other two molecules (Fig. 4*A*). Such a result highlights the fine sensitivity of ^{1}H chemical shifts in reporting local conformational deviations. ^{1}H NMR chemical shifts show an established correlation with secondary structure only for H^{α} resonances (35). None of the $\Delta\delta$ values of Fig. 4 alter the secondary structure profile inferred from the NMR chemical shift deviations of wild-type β_2-m with respect to the limiting values of statistically disordered conformations. In other words, the addressed variants adopt the same secondary structure as the parent sequence. This conclusion is felt to hold true also for the unassigned segments of H31Yβ_2-m, after considering the substantial persistence of the tertiary structure in the whole molecule, as inferred from the very small variations of the backbone hydrogen chemical shifts with respect to wild-type β_2-m in all the remaining (assigned) regions.

NMR-based Modeling—NMR-restrained modeling was not possible for either the truncated form, ΔN3β_2-m, or the H31Y mutant. A peculiarity of the truncated form was the occurrence in solution of a second minor species in equilibrium with the main component (ratio $\cong$ 1:4), as suggested by the presence of a second resonance for 28 residues: 7–10, 22, 25, 26, 37, 38, 49, 50, 55, 60, 66–69, 78, 79, 81–85, 88, 89, 91, 93, and 95–97. The vast majority of the residues that revealed resonance splitting belong to β-strands and are located in the central part of the molecule (Fig. 5). The only exception was Trp-60 that is in the loop D-E. Unfortunately, the extent of the splittings (often limited, see Fig. S1 in the Supplemental Material) and the degeneracy of most resonances made impossible defining a precise structural distinction between the two forms that were responsible for signal doubling pattern. Because of the presence of two different conformations, a proper quantitative analysis of the NOESY data was not viable, and therefore only qualitative inference could be drawn from the evidence on ΔN3β_2-m.

No NMR-based restrained modeling was attempted for

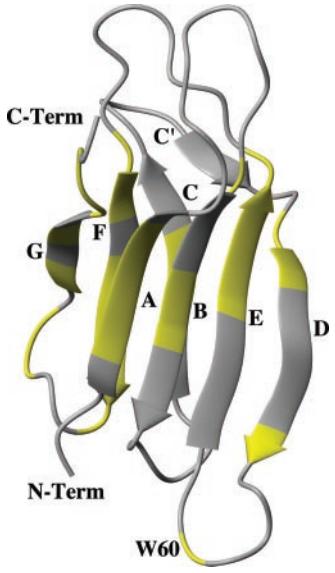

FIG. 5. **Ribbon model of ΔN3β_2-m backbone, based on wild-type β_2-m structure in water (5) according to the corresponding limited $\Delta\delta H^{\alpha}$ values (Fig. 4*A*).** The *yellow* tracts highlight the residues of the truncated variant for which resonance doubling was observed in the NMR spectrum. The plot was drawn using MOLMOL (27).

H31Yβ_2-m either, in this case because of the lack of any data from the B-C and D-E loop segments. The NOESY pattern of the mutant was largely superimposable to the corresponding data of wild-type sequence for the assigned resonances, which would have led to close conformational restraining, whereas no assessment at all was possible for the two mentioned loop regions where deviations could conceivably have emerged. Hence there was no point in running restrained modeling without any information from those loop regions. NMR restraints were instead collected and employed with R3Aβ_2-m. The structural inference from the substantial similarity between wild-type and mutant chemical shifts for both H^N (data not shown) and H^{α} (Fig. 4*A*) led us to use a tethered modeling approach in

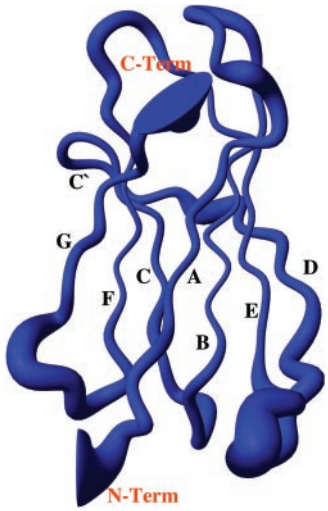

FIG. 6. **View of the 20 best-fitting solution structures of R3Aβ_2-m based on NMR restraints and tethered MD.** Only the C^α trace is drawn without side chains. The local trace *thickness* corresponds to the spatial spreading over the best overlap of the structural family ensemble. Only the first members of the solution structure families were considered. Plots were drawn with MOLMOL (27).

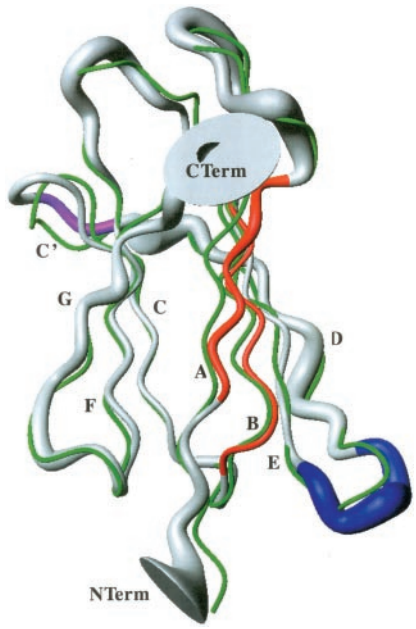

FIG. 7. **C^α trace overlap of wild-type β_2-m structure in MHC-I crystal (*green*) (39) and in solution (*gray*) (5).** The latter is the 20-member conformational family obtained from NMR-restrained MD, drawn with a thickness corresponding to the spatial spreading within the ensemble superposition. The *hot spots* in the solution structure, *i.e.* the deviations from crystal structure that represent the prodromes of the amyloid transition, are *highlighted* in different *colors* and correspond to strands A and B (*red*), strand C′ (*violet*), and loop D-E (*dark blue*). The graph was drawn with MOLMOL (27).

which all atoms within fragments 8–26, 38–52, 65–81, and 92–99 were kept fixed while restraining the remaining ones. With a starting point chosen from the 20 best conformers that were determined for wild-type β_2-m, the tethered MD run used 280 experimental distance restraints (129 intraresidue and 151 inter-residue), for residues 0–7, 27–37, 53–64, and 82–91. The restraints came from data that had been collected within 36 h from sample preparation. It is worth noting that, for the same region of the wild-type protein, 485 restraints could be employed. Despite this restraint number reduction, the resulting new family of R3Aβ_2-m conformers showed a pairwise global root mean square deviation (r.m.s.d.) for the backbone atoms of 1.50 ± 0.23 Å. The analysis of the spreading within the family revealed that, besides the N-terminal region (0–7), the loop between strands D and E was the most dispersed region, followed by the loop between strands F and G (Fig. 6).

The spreading extents, however, were distinctly larger than the corresponding ones observed within the structure family of wild-type β_2-m in solution (Fig. 7). A comparison between the mean structures from the 20 best-fit conformer families of wild type and R3A mutant showed a displacement maximum again in the loop D-E (r.m.s.d. 2.41 Å), with substantial deviations in the N-terminal region (r.m.s.d. 1.19 Å), loop F-G (r.m.s.d. 1.19 Å), and loop B-C (r.m.s.d. 0.49 Å). The smaller number of experimental restraints with respect to wild-type β_2-m was certainly determining for the latter outcomes (conformational dispersion and displacements), but reflected inherent definition limits of R3Aβ_2-m conformational distribution rather than defective restraining, as suggested by comparison with the wild-type protein nuclear Overhauser effect data set.

Precipitation Studies—A general feature of β_2-m solutions is the limited stability leading to precipitation of amorphous or/and fibrillar material over variable time periods. Protein precipitation depends on several factors, including pH, chaotropes, temperature, organic cosolvents, etc., that would deserve each one a specific analysis in the particular and unique context of amyloidogenic proteins. For β_2-m precipitation, sets of data obtained under different experimental conditions are available (36–38). Further systematic exploration is still necessary, however, because no comprehensive rationale has yet emerged. Moreover, a general caveat concerns the careful control of the initial protein preparation that may affect the experimental reproducibility of the precipitation studies. In our hands, for instance, sometimes different batches of wild-type β_2-m showed, under similar conditions, a remarkable diversity of precipitation pattern. Precipitation started within a few days when the initial solution was not clear, as a result of poorly soluble particles that catalyzed the process acting as seeds. By repeating the refolding procedure, the protein could be recovered and gave clear solutions without any early precipitation problem. In the present study, the typical conditions that support stability of β_2-m solutions for 1 month at least ($T \leq 310$ K, pH = 6.6, 100 mM NaCl, 70 mM phosphate buffer, 0.7–1 mM protein concentration) were tested with the three variants under investigation. For the truncated species, a clear tendency to precipitate was observed only with the freshly prepared, unfiltered solution. Centrifugation and filtering gave a stable sample, *i.e.* without any visible precipitate over a long time period (~1 month). An analogous filtration-dependent precipitation pattern was observed with H31Yβ_2-m. Even after initial centrifugation/filtration, however, a precipitate was formed, and the spectrum of H31Yβ_2-m soluble species appeared to deviate, over a 2-week time period, from the initial pattern, *i.e.* that typical of the structured protein. This time span was approximately halved without any initial treatment of the sample. Because the stability of any β_2-m variant solution is crucially dependent on the presence of insoluble protein material, the earlier precipitation observed with H31Yβ_2-m solutions compared with wild-type protein, despite the increased folding stability of the mutant, suggests that the preparation of H31Yβ_2-m is quite critical. Probably formation of poorly soluble adducts becomes more prominent with the slight hydrophobicity increase of the His-to-Tyr mutation.

Unlike the truncated variant and H31Y mutant, the solutions of R3Aβ_2-m were observed to last more briefly than those of wild-type protein at similar concentration. In particular, R3Aβ_2-m dissolved very quickly to give clear solutions, but

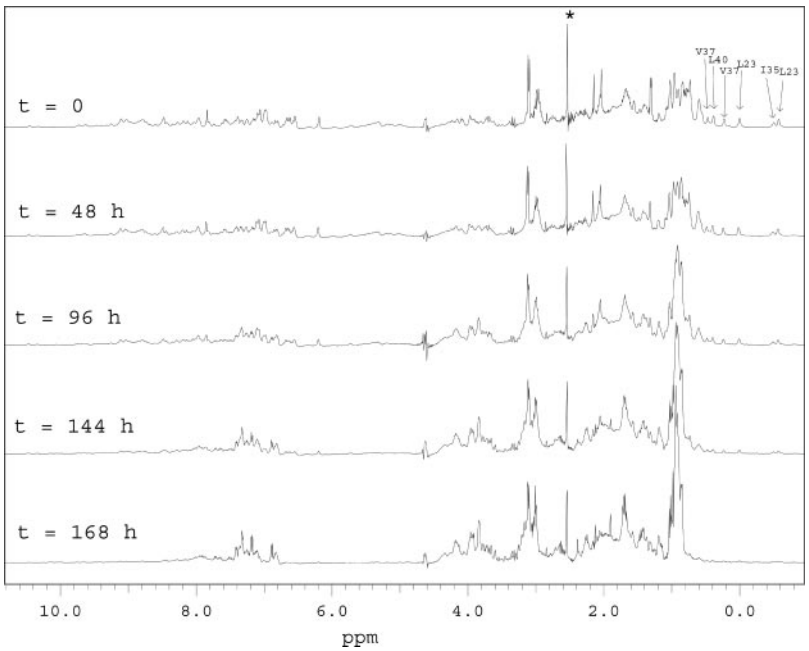

FIG. 8. **Time evolution of one-dimensional 500-MHz ^{1}H NMR spectrum of ~1 mM R3Aβ_2-m at 310 K.** The resolved signals with characteristic upfield chemical shift, after a lag phase of 24–36 h decrease with time and enable monitoring the loss of folded protein caused by precipitation and unfolding. The latter can be appreciated from the increase of resonance clustering in the disordered peptide regions. The *starred peak* identifies an impurity.

after 24–36 h (lag phase) started to show floating particles. This behavior was qualitatively independent of concentration and filtration, performed even though the starting solution appeared clear. A 5–6-fold reduction of R3Aβ_2-m concentration (0.15–0.2 mM) led, in fact, only to a corresponding lengthening of the lag phase and subsequent precipitation duration. At ~1 mM, precipitation was monitored to occur continuously and reproducibly over periods of ~7–8 days after the initial 24–36-h lag phase. NMR spectra taken at regular intervals showed, however, that, besides precipitation, the decrease of the structured protein signal was also the result of the onset of new resonances that clustered in the disordered peptide regions (Fig. 8). Thus, the mutant R3Aβ_2-m underwent also an unfolding process leading to a soluble species. The detection of soluble species coming from unfolding of native structure after observing precipitation seemed to be the rule among the addressed β_2-m derivatives, although the unfolding extent and the observed signal intensity thereof could vary. The loss of the structured species resonances, as well as the onset of new resonances from the soluble unfolded species, were followed by either one-dimensional and two-dimensional NMR measurements with R3Aβ_2-m, initially in an attempt to identify specific regions of the molecule with different rates of unfolding. No such region was found by treating the data on either an absolute or a normalized scale, *i.e.* using the integral (volume) of an entire representative spectral moiety as normalization factor. In addition to the resolved upfield-shifted resonances (the signature of any structured protein) that could be followed also in one-dimensional spectra, a number of resolved two-dimensional cross-peaks originating from the folded structure were analyzed and, after the initial lag phase, observed to decrease with the same rate throughout the considered time span.

Fig. 9 depicts the amplitude time course of some characteristic methyl resonances of folded R3Aβ_2-m. Following the initial lag phase, the loss of the structured species signal exhibits a linear trend, *i.e.* a concentration-independent behavior that corresponds to a pseudo-zeroth order kinetics. Analysis of the newly growing signals could only be performed within a restricted area of the two-dimensional fingerprint region, corresponding to the amide connectivities of statistically disordered peptides (see Fig. S2 in the Supplemental Material). After the initial latency, the onset rates proved to be quite scattered. This, most conceivably, should reflect the variable overlap extents and stoichiometries of the measurable cross-peak volumes from the unfolded species. Because no assignment was obtained for any of the new cross-peaks, the onset-rate data were not considered further.

pK_a Values—A calculation of pK_a values of ionizable residues was conducted for β_2-m, R3Aβ_2-m, and H31Yβ_2-m. The solution structure of β_2-m exhibits a number of deviations with respect to the x-ray conformation (Fig. 7) that may be related to the solvation of areas which are buried in the HLA complex (5). We investigated therefore the electrostatic properties of β_2-m using both the solution structure ensemble (5) (referred to as β_2-m_nmr), and the crystal structure of HLA complex (19), either with or without the heavy chain (referred to as β_2-m_HLA or β_2-m_X-ray, respectively). Hence the solvation effects, computed by a continuum model, were estimated for either solid-state structures, corresponding to an *in silico* solvent transfer, and for the solution ensemble. On considering the 20 best-fitting members of the solution structure family, the individually determined parameters related to the electrostatic properties were averaged.

In the case of R3Aβ_2-m, the input structures for UHBD calculations were based on the family of conformers determined by restrained dynamics. In the absence of a NMR-restrained structure of H31Yβ_2-m, the relative UHBD calculations were performed on a model that was built based on the wild-type protein solution ensemble, in consideration of the persistence of secondary and tertiary structure inferred from the backbone chemical shifts (Fig. 4*B*).

Table II summarizes the UHBD pK_a values, and Fig. 10 provides their comparison in the region that appears always relevant for stability. A number of residues in β_2-m_HLA showed unusual pK_a values that could be ascribed to the effect of inter- or intramolecular hydrogen bonds or salt bridges. The same holds for β_2-m_X-ray and β_2-m_nmr because of intramolecular H-bonds or salt bridges. Our attention was focused particularly on the pK_a variation of the histidines, the only residues whose acid-base equilibrium could be affected at experimental pH values around neutrality. Upon elimination of the MHC-I heavy chain, the computed solvation effects extend over the whole β_2-m surface. In response to such a change, the pK_a of H13 remained around a value close to the reference one

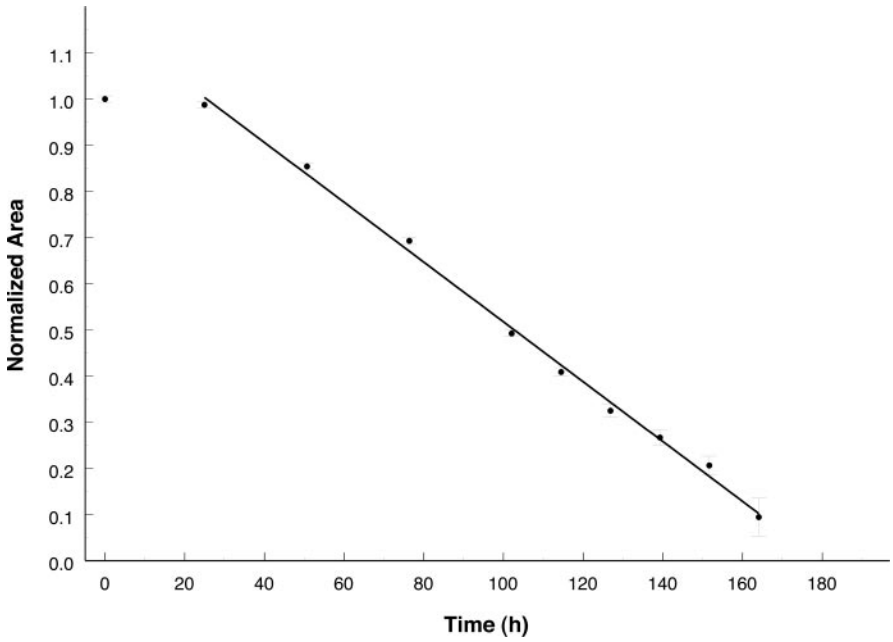

FIG. 9. **Amplitude time course of the characteristically upfield-shifted methylresonances of Leu-23 and Ile-35 from the ^{1}H NMR spectrum of R3Aβ_2-m.** Because the corresponding signals overlap partially, a single cumulative integral was measured. Following the initial lag phase, the signal loss exhibits a linear trend, *i.e.* a concentration-independent behavior that corresponds to a pseudo-zeroth order kinetics.

TABLE II

Calculated pK_a values of ionizable residues of wild-type and mutant β2-m species at 310 K

UHBD calculations on β_2-m were performed using (i) the crystal structure of MHC-I (39), with the heavy chain (β_2-m_HLA), (ii) without the heavy chain (β_2-m_X-ray), and (iii) the NMR solution structure ensemble (β_2-m_nmr). The experimental NMR solution structure ensemble was also employed for R3Aβ_2-m, whereas a model based on wild-type structure family in solution was used for H31Yβ_2-m. For the solution structure ensembles, the average pK_a values are given with the corresponding standard deviations. Values in italics indicate that the residue is involved in hydrogen bonds or salt bridges with residues of the HLA heavy chain. Values in bold indicate the presence of intramolecular salt bridges. Asterisked values indicate $\Delta pK_a \geq |0.4|$ of a mutant with respect to wild-type protein NMR ensemble. The reference side-chain pK_a values in unfolded protein used for calculation are: Arg = 12.0, Lys = 10.4, His = 6.3, Asp = 4.0, Glu = 4.4, and Tyr = 9.6.

Residue	β_2-m_HLA	β_2-m_X-ray	⟨β_2-m_nmr⟩	⟨R3Aβ_2-m⟩	⟨H31Yβ_2-m⟩
Met-0	7.68	7.28	7.36 ± 0.19	7.56 ± 0.24	7.4 ± 0.2
Arg-3	*14.64*	13.49	12.79 ± 0.33		12.6 ± 0.2
Lys-6	*12.29*	10.73	10.90 ± 0.29	11.30 ± 0.40*	10.8 ± 0.1
Tyr-10	*13.11*	10.16	10.17 ± 0.34	10.22 ± 0.37	10.2 ± 0.5
Arg-12	*14.17*	13.30	13.25 ± 0.55	13.12 ± 0.40	12.9 ± 0.3
His-13	6.05	6.25	5.72 ± 0.54	5.75 ± 0.49	5.9 ± 0.37
Glu-16	**3.09**	**2.87**	**3.76 ± 0.45**	**3.75 ± 0.48**	**4.0 ± 0.3**
Lys-19	**11.31**	**11.90**	**11.46 ± 0.47**	**11.38 ± 0.48**	**11.1 ± 0.3**
Tyr-26	12.26	10.05	10.29 ± 0.31	10.48 ± 0.58	9.9 ± 0.2
His-31/Tyr-31	*4.17*	5.26	5.41 ± 0.47	5.60 ± 0.46	9.8 ± 0.2
Asp-34	2.41	3.33	3.59 ± 0.13	2.84 ± 0.57*	3.7 ± 0.2
Glu-36	3.72	3.93	3.97 ± 0.39	3.90 ± 0.24	4.3 ± 0.3
Asp-38	**1.25**	**2.80**	**1.96 ± 0.47**	**2.20 ± 0.59**	**2.4 ± 0.5***
Lys-41	12.32	12.55	14.28 ± 1.39	14.35 ± 1.32	14.6 ± 1.6
Glu-44	4.32	4.26	3.39 ± 0.44	3.24 ± 0.54	3.6 ± 0.4
Arg-45	**14.41**	**13.49**	**13.46 ± 0.48**	**13.51 ± 0.45**	**13.4 ± 0.5**
Glu-47	3.87	3.96	3.83 ± 0.30	3.89 ± 0.28	3.8 ± 0.3
Lys-48	11.07	11.00	11.42 ± 0.35	11.35 ± 0.34	11.1 ± 0.1
Glu-50	4.16	4.19	3.92 ± 0.26	3.94 ± 0.24	3.9 ± 0.1
His-51	7.17	7.49	6.64 ± 0.16	6.72 ± 0.17	6.7 ± 0.2
Asp-53	*1.66*	3.68	3.41 ± 0.26	3.65 ± 0.19	3.7 ± 0.1
Lys-58	11.22	10.51	10.62 ± 0.09	11.19 ± 0.36*	10.7 ± 0.1
Asp-59	1.94	3.06	3.43 ± 0.27	2.77 ± 0.46*	3.7 ± 0.3
Tyr-63	*12.79*	10.15	10.62 ± 0.31	10.15 ± 0.17*	10.3 ± 0.2
Tyr-66	10.56	11.03	11.60 ± 0.38	11.59 ± 0.41	11.1 ± 0.2*
Tyr-67	11.97	11.02	10.63 ± 0.35	10.56 ± 0.34	10.7 ± 0.3
Glu-69	3.97	3.92	3.68 ± 0.36	3.78 ± 0.36	4.0 ± 0.1
Glu-74	3.85	3.86	4.03 ± 0.30	4.09 ± 0.28	4.2 ± 0.2
Lys-75	10.76	10.79	10.98 ± 0.32	10.94 ± 0.32	10.8 ± 0.1
Asp-76	2.52	2.34	2.06 ± 0.52	2.05 ± 0.56	3.0 ± 0.3
Glu-77	**2.66**	**3.12**	**3.23 ± 0.55**	**3.31 ± 0.54**	**3.7 ± 0.5***
Tyr-78	10.25	9.95	9.56 ± 0.45	9.65 ± 0.46	8.7 ± 0.6*
Arg-81	**14.03**	**13.31**	**13.60 ± 0.32**	**13.81 ± 0.33**	**13.3 ± 0.3**
His-84	3.60	3.96	4.14 ± 0.39	4.49 ± 0.65	4.8 ± 0.2
Lys-91	10.83	10.54	10.50 ± 0.13	10.55 ± 0.26	10.5 ± 0.1
Lys-94	**12.26**	**12.11**	**11.53 ± 0.50**	**11.44 ± 0.53**	**11.0 ± 0.3**
Asp-96	3.32	3.62	3.62 ± 0.37	3.71 ± 0.34	3.7 ± 0.4
Arg-97	13.76	13.56	13.62 ± 0.57	13.58 ± 0.63	13.2 ± 0.5
Asp-98	*1.95*	4.00	4.00 ± 0.26	3.97 ± 0.24	4.1 ± 0.2
Met-99	*0.55*	3.81	3.41 ± 0.52	3.48 ± 0.44	3.5 ± 0.3

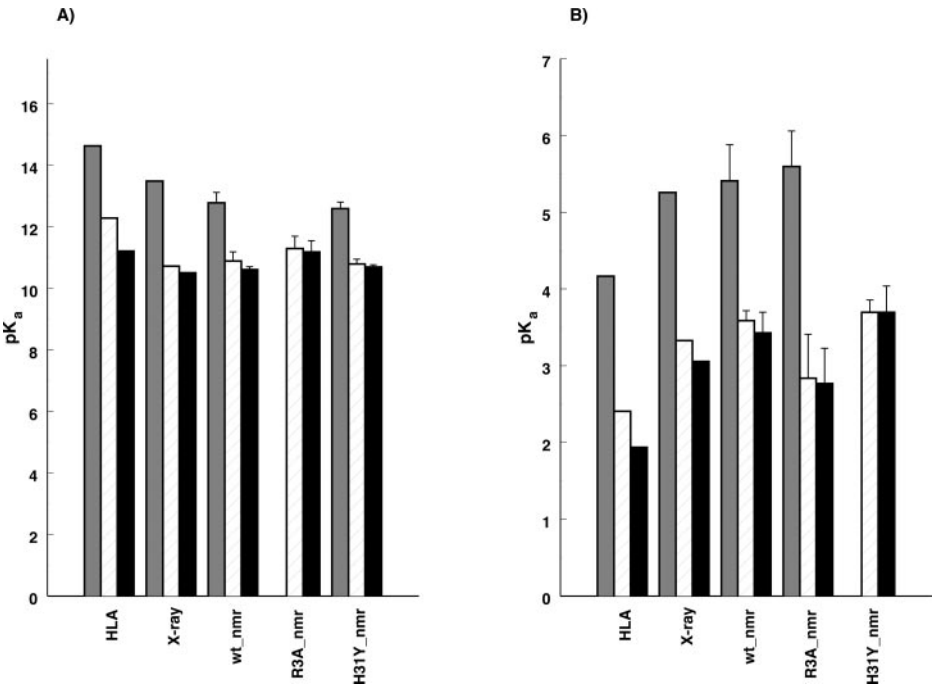

FIG. 10. **Calculated pK_a values for some residues of wild-type β_2-m in the crystal structure conformation (39), with (*HLA*) and without (*x-ray*) heavy chain, in the solution structure conformation (5) (*wt_nmr*), and in R3A and H31Y mutants (see text).** For each species the *left histogram* (*A*) depicts the pK_a values of Arg-3 (*gray bar*), Lys-6 (*hatched bar*), and Lys-58 (*black bar*), whereas the *right histogram* (*B*) reports the pK_a values of His-31 (*gray bar*), Asp-34 (*hatched bar*), and Asp-59 (*black bar*). The *error bars*, shown for NMR structures, represent the standard deviation over the considered conformational ensemble.

(see Table II), wherever the considered structures came from, *i.e.* X-ray data or NMR determinations. His-31, the side chain of which in the complex experiences a salt bridge with the heavy chain counterpart, shifted its pK_a value from 4.17 to 5.26 in β_2-m_X-ray, *i.e.* within the standard deviation of the average value of 5.41 obtained with β_2-m_nmr (Table II), where the original orientation also proves changed toward a more outward-pointing geometry (5). His-51 showed minor variations of pK_a, always close to the reference value, whereas His-84, which maintains the imidazole ring always embedded in the core of the protein, conserved an unusually low pK_a value in any of the considered structures.

The pK_a values computed for R3Aβ_2-m were largely similar to those obtained for β_2-m_nmr, including the general trend of the histidine residues. Residues such as Lys-6, Asp-34, Lys-58, Asp-59, and Tyr-63 were predicted to display conspicuous deviations (more than 0.4 pK_a units, Table II) without any relevant effect, however, on the total molecular charge at the experimental pH value of 6.6. An interesting feature was the small pK_a increase estimated for His-31 with respect to the corresponding value of wild-type protein in solution, *i.e.* 5.60 *versus* 5.41. Despite the limited extent, this change is significant and in line with the expected trend. By mere substitution of alanine for arginine in position 3 of wild-type protein solution ensemble, an average pK_a increase of 0.7 units could be calculated for His-31 that should represent exclusively the variation resulting from the drop of the positive charge at the mutation site. The conformational contributions conveyed by the solution ensemble of R3Aβ_2-m balance the 0.7 units pK_a increase of His-31, but only in part. As a result, the residual small pK_a increase of His-31 should affect the molecular charge under the experimental pH conditions.

The effect of the mutation of histidine in position 31 with a tyrosine were estimated to cause remarkable shifts on pK_a values of Asp-38, Tyr-66, Asp-76, Glu-77, Tyr-78, and Lys-94 with respect to the corresponding values in wild-type solution structure. Besides the slight decrease of positive charge as a result of the direct consequence of the mutation, these shifts should contribute again no additional major molecular charge variation near neutrality conditions.

Electrostatic and Solvation Contributions to Free Energy—Unfolding free energy can be split into an electrostatic, pH-dependent term, and a non-electrostatic term. The electrostatic contribution to the folded form free energy is directly related to pK_a values according to the equation described by Yang and Honig (40). Analogously, for the unfolded form, a similar computation can be performed assuming that the pK_a values of ionizable groups in denatured state are identical to those obtained for isolated amino acids.

In Table III, the calculated $\Delta G_{el}^{F\text{-}U}$ values are listed for wild-type β_2-m (either crystal and solution structure) and the two investigated mutants, along with the experimental global unfolding ΔG values. A direct comparison of calculated and experimental free energy differences is not feasible because the experimental ΔG values of unfolding include the non-electrostatic contributions. A more sensible parameter is $\Delta\Delta G_{el}^{F\text{-}U}$ with respect to wild-type species, when compared with the corresponding experimental $\Delta\Delta G$. The computed data show a higher electrostatic contribution to stability for both mutants with respect to wild-type protein and a reduced electrostatic contribution for β_2-m_X-ray. The latter cannot be directly compared with experimental values, but could be considered to account for the rearrangements the protein undergoes in solution leading to an increased electrostatic stabilization. A similar rationale cannot be applied directly to the other results of Table III because of the starting charge differences between wild-type and mutants. Hence the $\Delta\Delta G_{el}^{F\text{-}U}$ values obtained for both mutants can no longer be interpreted only in terms of local conformational differences with respect to the natural sequence.

For His-31Yβ_2-m, the increased thermodynamic stability expressed by the experimental $\Delta\Delta$G of unfolding is in qualitative agreement with the computed increase of electrostatic contribution to free energy. On the other hand, the computed $\Delta\Delta G_{el}^{F\text{-}U}$ value for the mutant R3Aβ_2-m indicates that the electrostatic contribution can hardly account for the experimental $\Delta\Delta G$ of unfolding of the species.

To take into account hydrophobic interactions between the protein and the solvent, which contribute to the non-electrostatic terms of free energy, a calculation of the solvation component (ΔG_{sol}) in the factorization of global unfolding ΔG was undertaken. The procedure to calculate ΔG_{sol} values entails defining a reference state, typically the unfolded state, and hence introduc-

TABLE III

Calculated electrostatic and solvation contributions to free energy differences compared with experimental unfolding free energies

The experimental data obtained for solutions of β_2-m, R3Aβ_2-m, and H31Yβ_2-m are compared with the calculated values for the NMR structural families, averaged over the ensemble of 20 best-fitting conformations, or the crystal structure of β_2-m in MHC-I. Only for H31Yβ_2-m were calculations performed on a model that was built based on the wild-type protein solution ensemble. All values are in kcal/mol.

	Experimental[a]		Calculated[b]		
	ΔG	$\Delta\Delta G^c$	$\Delta G_{el}^{F\text{-}U}$	$\Delta\Delta G_{el}^{F\text{-}U}$[d]	$\Delta\Delta G_{sol}$[e]
β_2-m_X-ray			7.5	−1.8	34 (±13)
$\langle\beta_2$-_nmr$\rangle$	6.3 ± 0.2		9.3 ± 1.3		
$\langle$R3Aβ_2-m$\rangle$	5.9 ± 0.2	−0.4	10.1 ± 2.1	0.8	72 ± 31
$\langle$H31Yβ_2-m$\rangle$	7.8 ± 0.4	1.5	13.1 ± 2.1	3.8	−1 ± 26

[a] Unfolding free energies were determined at pH = 7.3 and T = 293K (see Table I).
[b] $\Delta G_{el}^{F\text{-}U}$ represents the electrostatic contribution to unfolding ΔG calculated with UHBD program at 293 K and pH = 7.5.
[c] The differences are determined with respect to the experimental value obtained for wild-type β_2-m.
[d] The differences are determined with respect to $\Delta G_{el}^{F\text{-}U}$ calculated for $\langle\beta_2$-m_nmr$\rangle$.
[e] The values are the differences between the ΔG_{sol} of the crystal structure conformation (β_2-m_X-ray) or the average ΔG_{sol} calculated over the solution structure ensemble (R3Aβ_2-m and H31Yβ_2-m) and the average ΔG_{sol} obtained for β_2-m_nmr, *i.e.* over the 20 best-fitting solution conformers of β_2-m. Note that, in contrast to $D\Delta G_{el}^{F\text{-}U}$ and global $\Delta\Delta G$ of unfolding, a positive $\Delta\Delta G_{sol}$ value indicates destabilization with respect the solution structure of β_2-m because the solvation free energy differences (ΔG_{sol}) between unfolded and folded states are negative.

ing arbitrary assumptions related to precise description of unfolding. If the same protein is considered in different conformations, however, only $\Delta\Delta G_{sol}$ values are actually needed and thus the computations for whichever reference state is unnecessary, by definition. By analogy, a similar advantage can be exploited to compute $\Delta\Delta G_{sol}$ for proteins that differ by a single residue. To deal with point mutations of β_2-m sequence into R3Aβ_2-m and H31Yβ_2-m, the individual contributions to ΔG_{sol} because of the hypothetical reference state of Ala-3 or Arg-3 and His-31 or Tyr-31 were suppressed by subtracting their contributions, ΔG_{sol}^{un}, in linear tripeptides G*X*G, where *X* stands for Ala, Arg, His, or Tyr. Accordingly, the differences were calculated as follows: $\Delta\Delta G_{sol}$(R3Aβ_2-m − β_2-m_nmr) = [ΔG_{sol}(R3Aβ_2-m) − ΔG_{sol}^{un}(GAG)] − [ΔG_{sol}(β_2-m_nmr) − ΔG_{sol}^{un}(GRG)], and $\Delta\Delta G_{sol}$(H31Yβ_2-m − β_2-m_nmr) = [ΔG_{sol}(H31Yβ_2-m) − ΔG_{sol}^{un}(GYG)] − [ΔG_{sol}(β_2-m_nmr) − ΔG_{sol}^{un}(GHG)].

According to the atomic solvation parameters methods (31), the solvation free energy that is based on parametric atomic solvation parameters takes into account electrostatic and nonelectrostatic terms. Table III reports the average values of $\Delta\Delta G_{sol}$ for R3Aβ_2-m, H31Yβ_2-m, and β_2-m_X-ray with respect to β_2-m_nmr. Positive values of $\Delta\Delta G_{sol}$ indicate a destabilizing contribution from solvation compared with β_2-m solution structure. This destabilization seems to affect both the heavy chain-bound conformation of wild-type protein and the R3A mutant. The result agrees with expectation for β_2-m_X-ray, while suggesting, in the case of R3Aβ_2-m, that the stability difference of this mutant compared with wild-type sequence could be ascribed to a less favorable solvation contribution, on considering the corresponding $\Delta\Delta G_{el}^{F\text{-}U}$ value. Finally, the negligible difference between ΔG_{sol} of H31Yβ_2-m and β_2-m is consistent with a mutant model that was built based on the wild-type protein solution ensemble, a conflicting bias for the assessment of solvation free energy differences and corresponding contributions to global $\Delta\Delta G$.

DISCUSSION

Stability and Structure of β_2-m: Variants Versus Wild Type—The solution structure of human β_2-m, determined by ^{1}H NMR spectroscopy and restrained modeling calculations (5), exhibits several deviations compared with the crystal structure of the protein associated to MHC-I heavy chain component (Fig. 7). These structural differences can be considered as the prodromes of the amyloid transition. Solvation of the protected regions in MHC-I leaves β_2-m molecule in a poorly stabilized state, where even minor charge and solvation changes, in response to pH or ionic strength variations, can easily compromise the hydrophobic/hydrophilic balance and drive a transition to relieve the hydration stress. This transition should imply unpairing of strand A and should lead to polymerization into fibrils or amorphous aggregates and, eventually, precipitation (5, 6). The same mechanism can account for the partial unfolding and fiber formation subsequent to Cu^{2+} binding, which was shown to occur primarily at His-31 and involve partially His-13 as well, the next available His residue along the transition pathway (5).

The solvation sensitivity of β_2-m surface at the interface with the heavy chain of MHC-I was first recognized after realizing that the extended hydrophobic patch embedding the four positive charges of Arg-3, Lys-6, Lys-58, and Lys-91 (spread over the surface shown in Fig. 7) had to release the MHC-I packing (39) and accommodate some mobility of the charged side chains to supply a favorable contribution to free energy (6). The lack of such a contribution and the ensuing instability (Table I) could explain the properties and behavior of fragment ΔN6β_2-m observed *in vitro* (7, 6). *In vivo* the same fragment accounts for ~30% of the protein material in β_2-m fibrils and could originate from proteolysis (41), once strand A detachment from sheet 1 has made accessible and mobile the N-terminal segment, in agreement with the amyloid transition pathway already described. Although the exact timing of ΔN6β_2-m formation, *i.e.* whether prefibrillar or postfibrillar, is not yet established, the available data on structure and the mild conditions used for fibrillogenesis, along with the results from limited proteolysis (6, 41), strongly indicate that the species can be considered the closest representation of the amyloidogenic conformation of β_2-m.

To check further the solvation sensitivity-driven mechanism outlined above, the variants ΔN3β_2-m and R3Aβ_2-m were designed and characterized. The unfolding free energies were intermediate between the values of wild-type and fragment ΔN6β_2-m (Table I), confirming that the positive charges on the N-terminal strand are a stability factor for the isolated protein. Compared with ΔN6β_2-m, the fragment ΔN3β_2-m does not exhibit quick precipitation and, based on the $\Delta\delta H^\alpha$ values (Fig. 4*A*), its structure in solution should remain quite similar to that of the parent protein over relatively long periods (weeks), without any hint of increased aggregation as observed with the shorter fragment (6). The occurrence of two different conformers, in slow exchange on the NMR time scale (Fig. 5 and Supplemental Material, available in the on-line version of this article), does not seem to affect this conclusion. In response to loss of the N-terminal tripeptide, it is likely that the fragment ΔN3β_2-m is capable of arranging in solution a vicarious role of the N-terminal amino group of Met-0, which is located close to the former location of the missing Arg-3 residue. The importance of the positive charge at position 3 to complement the

number of positive charges inserted in a surface hydrophobic patch is highlighted by the results obtained with R3Aβ_2-m. Apparently its NMR solution structure exhibits limited variations with respect to the wild-type protein, mostly clustered at the D-E loop, but the samples do not last more than a couple of weeks as a result of precipitation and unfolding. The thermodynamic stability of R3Aβ_2-m mutant is higher than that of the examined truncated variant, ΔN3β_2-m, because of the additional N-terminal tripeptide of the mutant and the conceivable free energy contributions thereof. On the other hand, the absence of the positive side chain at position 3 in R3Aβ_2-m brings about a small but significant destabilization with respect to wild type that should be ascribed to the hydrophobic solvation contribution, according to the earlier interpretation (6). The calculated values from theoretical dissection of the unfolding free energy confirm the expectations. From Table III it is clear that the destabilization of R3Aβ_2-m with respect to wild-type protein is not because of the electrostatic term (that, instead, appears to stabilize slightly), but to the solvation term. The result, albeit only qualitative, is valuable because experimentally reliable if one considers that it was obtained from the NMR-based conformational family of R3Aβ_2-m. The effects of the altered solvation term, which can nicely account for the decreased stability of R3Aβ_2-m, should not be confined only to the mentioned hydrophobic surface. Other sensible surface areas are the loops B-C and D-E, the end of strand D and the start of strand E, all located on the side of the N terminus of the protein, above the extended hydrophobic patch region (Fig. 7). In particular, exposed surface changes must be certainly involved at His-31 side chain, orientation change (5) and pK_a increase (Table II) of which can be directly related to an increase of the local positive charge, at neutral or slightly acidic pH, and loss of packing with the N-terminal residues of strand A. This mechanism, although contributing to destabilization of R3Aβ_2-m with respect to wild-type protein, as inferred from the corresponding His-31 pK_a value (Table II), should be considered the basic one to accelerate strand A detachment from sheet 1 upon further increase of His-31 positive charge by either pH decrease or Cu^{2+} binding (5). Because the link between Cu^{2+} binding and partial unfolding of β_2-m is the local charge increase on His-31, equivalent to acidification of a neutral β_2-m solution, to design a more stable protein we reasoned that a mutant His-31→ Tyr might prevent the destabilizing imidazole titration, while preserving the local aromatic character. The expectation was successful as the designed mutant has been shown to display increased folding stability relative to the wild-type protein (Table I), along with reduced Cu^{2+} binding (42). Although the His-31-mediated mechanism for Cu^{2+} specificity was judged reasonable, an additional, alternative view was advanced involving a copper binding site in nonnative (unfolded) β_2-m states (32). The issue would deserve further consideration, out of the scopes of the current work, but it is worth noting here that the crucial role of His-31 for the stability of isolated β_2-m is confirmed by the intermediate stability of mutant His-31 → Ser, more stable than wild-type β_2-m as a result of absence of positive charge at Ser-31, but less stable than H31Yβ_2-m because of the decreased hydrophobic character of the same residue. That the main contribution to H31Yβ_2-m stabilization comes from the loss of positive charge at the mutation site follows also from theoretical results of Table III. The electrostatic contribution to free energy accounts for the whole stability gain of the mutant, with no resulting solvation contribution. Although the results for H31Yβ_2-m may be biased by the specific conformation chosen for calculations (modeled from the wild-type ensemble in solution), recent x-ray structural evidence are in fairly good agreement with the conformational features imposed to H31Yβ_2-m solution structure (43). Thus, no incorrect conformational bias should affect the computed free energy components of Table III.

The increased stability of H31Yβ_2-m compared with wild type and R3Aβ_2-m has also been related to the different rates of conformational exchange occurring at the D-E loop. Indeed the dynamics at this loop, which can only be inferred indirectly from NMR data, are an additional facet of the solvation arrangement that β_2-m and variants thereof reach in aqueous solution. In MHC-I, in fact, loop D-E and the contiguous strand segments of β_2-m are also part of the interface between the two proteins of the complex (39). The analysis of unfolding and refolding kinetics of H31Yβ_2-m reveals features similar to those reported for wild-type β_2-m (14). Clearly the slower rate of unfolding measured for the mutant with respect to wild type correlates with the increased stability of the former. On the other hand, the increased rate of the slow refolding phase measured for both H31Y and H31S mutants can be tentatively interpreted, based on the rearrangement of the hydrophobic core observed to occur in wild-type protein during the same phase (Fig. 2). Both mutants bear a sequence change at His-31, an extremely critical residue for the consequences of its pK_a variation. This type of variation is intimately linked with local conformation changes. Besides considering the related effects on the solvation and packing of the N-terminal moiety of strand A, it is worth remembering that the orientation of the imidazole group in the solution structure of wild-type β_2-m (5) is distinctly different from the corresponding orientation in MHC-I crystal (39). This should affect the neighboring Phe-30 and, in turn, the packing of the latter with Ile-35, *i.e.* residues involved in the complex, and probably cooperative, rearrangement of the hydrophobic core undergone by the protein during refolding (Fig. 2). Hence, it should not be surprising that mutations at His-31 may influence the rearrangement process and its kinetics. In particular, because both H31Y and H31S mutants are more stable than wild type and exhibit a faster slow phase-refolding rate (Fig. 3), it should be concluded that their I_2 intermediates are closer to the final structure (or the transition state toward it) and thus reach it more easily than wild-type protein, because of the effects of the mutations in position 31. Although this may be the result of different scenarios, at least for H31Yβ_2-m the available structural evidence (43) could suggest that an orientation of Tyr-31 side chain similar to that of β_2-m in MHC-I (39) may greatly facilitate the hydrophobic core rearrangement and therefore speed up the final step of refolding.

To summarize, a thorough analysis of the structure and stability of two β_2-m mutants, R3A and H31Y, along with additional data from a truncated variant, ΔN3β_2-m, and another mutant, H31S, fully support the plausibility of an amyloidogenic pathway of β_2-m based on recognition of the transition prodromes from the solution structure of the isolated protein (5, 6). The results of a systematic investigation on 13 amyloidogenic β_2-m mutants have recently been published (44, 45). Although no correlation was proposed between the location of the mutations and the extent of destabilization with respect to wild-type sequence, a unique role in amyloid formation was envisaged for the N and C-terminal β-strands of β_2-m (A and G, respectively) from the increased fibrillogenesis rate at acidic and mildly acidic pH of the variants with mutations in strands A and G. The underlying rationale is based on the loss of local hydrophobic packing by β-strand unpairing, leading to increased population of conformers with exposed assembly-competent surfaces. By different arguments, from previous (5, 6, 41) and present evidence, we have proposed that detachment of strand A is the crucial event leading to intermolecular pairing

of β_2-m. Because the terminal β-strand unpairing and the subsequent local mobility increase should enhance proteolytic cleavage at the N-terminal, as already mentioned (6, 41), as well as at the C-terminal β-strand of wild-type β_2-m sequence, we note that the terminal strand unpairing appears more likely to occur at the N terminus because of the much higher abundance of N-terminally truncated species (>30%) than C-terminally truncated ones (<1%) in natural fibrils (7).

On the Amyloid Transition—The experimental and theoretical results obtained with the examined variants of β_2-m confirm, overall, the important role that charge and solvation changes assume in determining the stability of the protein. Besides the extended hydrophobic patch interrupted by the positive charges of Arg-3 and Lys-6 (N-terminal region), Lys-58 (D-E loop), and Lys-91 (G strand), another potentially solvation-sensitive location is His-31 in the B-C loop. The inherently stressed structure of isolated β_2-m reacts to any charge and solvation modification at these *hot spots* by accelerating a transition, the amyloid one, which starts with unpairing and disordering of strand A and leads to intermolecular pairing through strands D and C and, eventually, to precipitation. Several lines of evidence have been accumulated in favor of this mechanism (5, 6, 8, 9, 41, 43, 46–48), which prompts some considerations concerning the amyloid transition of β_2-m. It is widely accepted, in fact, that amyloid formation proceeds through partial unfolding transformations of the parent protein, which reaches a crucial intermediate conformation that can either undergo further unfolding or become trapped into an intermolecular aggregation process (2). This alternative pathway leads eventually to precipitation: the fibrillar, amorphous, or mixed nature of the precipitate depending on the actual experimental conditions. Most generally, the mechanism does not necessarily imply the intermediate to be a metastable species, although it is much more than intuitive to postulate a metastable intermediate at any bifurcation point. It is clear that the more stable the intermediate, the easier its observation. Metastable intermediates may even be considered addressable targets, not necessarily for blocking the amyloid transition, but, rather, also for studying their properties to prevent the process. On the other hand, partial unfolding intermediates may also be very transient species. This indeed appears to be the case with β_2-m amyloid transition. No trace of stable intermediate species has ever been observed in the NMR spectra of either the wild-type or variant proteins here examined, whereas for the least stable and fastest fibril-forming variant of Table I, ΔN6β_2-m, only evidence of intermolecular association was obtained from gel filtration and NMR data (6). Extensively unfolded species were detected in conjunction with the observation of precipitates in R3Aβ_2-m and H31Yβ_2-m solutions, and similar results had been obtained occasionally also with some preparations of wild-type β_2-m, in particular when precipitation was observed to occur shortly after solution preparation because of the presence of insoluble particles. Quantitative measurements were limited to R3Aβ_2-m because of the particularly convenient time frame of the process in this mutant. The observation of soluble unfolded species always and only in the presence of precipitates, and the pattern of the structured protein resonance loss, which exhibits a clear lag phase and a pseudo-zeroth order kinetics (Fig. 9), suggest the occurrence of a pathway where the intermediate formation is a necessary, but most likely transient step, along the more complex and involved route of nucleated conformational conversion (NCC) (49–51). According to this mechanism, soluble, conformationally dynamic oligomers should undergo a nucleation transition, to form the assembly-competent species that grow into fibrillar aggregates. The nucleation event is the rate-determining step that should explain a lag phase because of the simultaneous and precise partial unfolding transition that a minimum number of monomers (the nucleation number, N_n) must undergo to establish a nucleus, whereas the lack of concentration dependence of the structured protein signal decrease (pseudo-zeroth order kinetics) should be the consequence of the direct dependence of the precipitation and unfolding rates on the actual concentration of the nucleated protein reservoir, a group of species that are largely unobservable by NMR as a result of their dimensions. As checked with R3Aβ_2-m, the increase of lag phase duration upon decreasing the protein concentration, and the accompanying slope reduction for the linearly decreasing part of the time-course function corresponding to the trend shown in Fig. 9, are in line with the expected pattern from a NCC-type mechanism (51). A nucleation-dependent polymerization model has already been proposed for β_2-m fibril formation *in vitro* and *in vivo*, based on kinetic data analysis (36). The present qualitative kinetic observations, while suggesting the extension of the NCC mechanism to β_2-m fibrillogenesis, also provide some clues that can be of general interest for amyloid transition of globular proteins. In particular, the link between unfolded species and precipitate, which was invariably seen in our experiments, suggests that extensive protein unfolding leading to soluble species should occur via release of properly unfolded monomers from the nucleated species, and irreversible, further unfolding of the same mono-

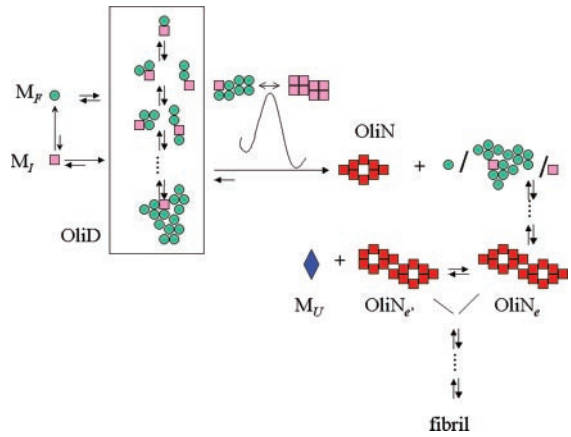

FIG. 11. **Proposed NCC-type mechanism (49–52) for β_2-m fibrillogenesis.** The rate-determining step is the conversion of the dynamic oligomer (OliD) into the nucleated oligomer (OliN) and entails a concerted transition by which N_n closely spaced monomers convert simultaneously into a nucleus of intermediates. This is highlighted by the pictorial representation of the transition state above the *arrows* of the rate-determining step. In general, OliD could be a series of aggregates with various stoichiometries or a series of adducts that are formed by association equilibria. OliD should be composed of either folded species (M_F) and conformationally activated or partially unfolded species (M_I). In the general scheme above outlined, M_I monomers are considered in equilibrium with M_F, *i.e.* as thermodynamic intermediates. However, M_I monomers, whether partially unfolded species or activated folded states, could also be transient species, *i.e.* kinetic intermediates. This latter nature of M_I could be the case with β_2-m based on the NMR evidence (Figs. 2 and 9), despite the former possibility (thermodynamic intermediate) cannot be definitely ruled out, as also suggested by previous results (15, 42). Once formed, OliN elongates by addition of M_F, M_I, or OliD and subsequent conformational rearrangement of the incorporated monomers. Elongated nuclei ($OliN_e$) keep growing to form eventually a fibrillar, amorphous, or mixed precipitate, but may also release partially unfolded monomers, in a conformational state other than M_I. These released species undergo irreversible further unfolding to reach a soluble unfolded state (M_U). Soluble unfolded species may be obtained, of course, also directly from partially unfolded or destabilized monomers, a route that is not necessarily alternative to the release from nucleated species, but may coexist. Note the different colors and arrangement of the monomers in the M_I nucleus and in OliN. The *symbols* indicate that different intra- and intermolecular conformational arrangements are adopted within the M_I nucleus and the fibril nucleus.

mers to remain in solution, according to the scheme of Fig. 11. The rate-limiting step (the dynamic-to-nucleated oligomer conversion) entails achieving the transient intermediate structure in N_n closely-spaced monomers within the conformationally dynamic oligomer. Rather than an aggregate with definite stoichiometry, the dynamic oligomer of β_2-m could most likely be one of the adducts along a series of ongoing association equilibria (6). The NCC mechanism is a general, flexible scheme, which can account for different specific aspects of a broad class of nucleation-based processes, as recently shown by Bitan and colleagues (52). No matter whether a proper oligomerization or an association equilibrium is involved, the onset of a population of conformers such as that observed by real-time NMR should facilitate strand A unpairing (6, 45) to provide the energetic pushing for the nucleation and the successive fibrillogenesis. From a thermodynamic viewpoint, this means that the stressed conformations of the associated β_2-m monomers in water overcome their (meta)stability barrier to reach a more stable state in the oligomer that nucleates through intermolecular β-strand pairing. As previously pointed out (53), this mechanism enjoys the relevant merit of providing a proper thermodynamic consistency to bypass the conformational inertia of the protein monomer in water.

The transient intermediate view we have just outlined is consistent with the previous reports concerning the occurrence of a monomeric β_2-m intermediate named I_2 and involved in fibrillogenesis (14, 15, 42). The I_2 intermediate was inferred from the analysis of the slow phase of the refolding kinetics and detected by circular dichroism and capillary electrophoresis at low protein concentration (1–40 μM) always along the refolding pathway of β_2-m. The data obtained by real-time NMR (Fig. 2) suggest that I_2 corresponds to a poorly stable fold of the protein, with a dynamic hydrophobic packing pattern that seems, however, to conserve substantially the tertiary topology of native β_2-m and to convert slowly into the latter. The fibrillogenic propensity of I_2 that was observed on addition of seeding to refolding β_2-m solutions (15, 42) is compatible with the NMR picture of a destabilized protein form undergoing an easier amyloidogenic transformation.

In the context of a NCC mechanism, the actual intermediate of β_2-m along the amyloid transition should be the nucleated oligomer. However, the possibility of transient intermediate(s) formation before the nucleation step should not be ruled out *a priori*. Within the NCC framework (49–51), the features of the dynamic oligomer are so loose that postulating monomers, already in partially unfolded conformation(s) or in a sort of activated state like the I_2 species described from NMR evidence, that occur either sporadically over the dynamic oligomer population, or even promote the same dynamic oligomerization being thus responsible for it, could fit the mechanism anyway (Fig. 11). The really qualifying aspect of the NCC scheme is the requirement for a concerted transition involving a precise number of closely spaced monomers, as opposed to the single molecule event. This means considering an ensemble of molecules before and after the transformation, and the thermodynamics thereof. Similar considerations extend also to the formation of unfolded soluble species. First, an oligomeric nature for the unfolded soluble species cannot be excluded. The above-used notation M_U stems from the NMR line sharpening, *i.e.* a qualitative argument, observed in solutions of R3Aβ_2-m, an ideally suited mutant to follow, within reasonably short periods, precipitation, and unfolding. Second, obtaining an extensively unfolded species in solution, whether monomeric or not, not only from the dissociation equilibrium of an elongated nucleus, could well be related to the presence of a partially unfolded intermediate prior to nucleation.

CONCLUSIONS

The NCC mechanism, which was demonstrated for Alzheimer Aβ peptide (49, 52) and Sup35 NM domain (50) and proposed as the most general and reliable scheme for amyloidogenesis (51), seems to apply also to β_2-m fibril formation. The NCC scheme is consistent with the experimental findings from the present study on structure, precipitation, and unfolding of β_2-m variants, along with the role of the previously identified amyloid transition prodromes of wild-type β_2-m (5) for the onset of a transient intermediate. The consistency extends also to the Goto group proposal concerning the dependence of β_2-m amyloidogenic potential on the mobility restrictions imposed by the single disulfide bridge of the molecule (47, 48). By reducing this disulfide bridge, the helical propensity of strand E takes over and spoils the quality of the intermolecular β-strand pairing that should occur at the adjacent D strand. On the other hand, by keeping the disulfide, a rigidity constraint is introduced at strand E, which prevents spoiling of the intermolecular pairing. The NCC scheme entails oligomer nucleation, which can take place only via intermolecular interactions. Polypeptide chains can maximize intermolecular interactions by establishing pairings between β strands of individual chains, to form sheets where the acid-base potential of backbone amide and carbonyl groups are satisfied intermolecularly. Conversely, polypeptides can maximize intramolecular interactions by adopting α-helical conformations where the same acid-base potentials are internally balanced. The result of the competition between inter- and intramolecular interactions, that, in turn, are competed anyway by solvent-polypeptide interactions, is determined by the specific amino acid sequence. Therefore, the amyloidogenic potential of any polypeptide chain could be ultimately related to its intramolecular interaction potential in water, *i.e.* the same potential that determines the overall folding in water. Exceptions to this scheme, such as intermolecular interactions established by individual helices, may well be possible, but the general character of the conclusions appears consistent with the unifying soundness of the NCC mechanism for amyloidogenesis, as suggested by recent results on the recognition of soluble oligomers of different amyloidogenic proteins by a single antibody, which also inhibits the corresponding *in vitro* toxicity (54).

Acknowledgments—G. E. thanks Dr. F. Al Piaz for helpful discussions and Dr. A. Makek for assistance.

REFERENCES

1. Merlini, G., and Bellotti, V. (2003) *N. Engl. J. Med.* **349,** 583–596
2. Dobson, C. M. (1999) *Trends Biochem. Sci.* **24,** 329–332
3. Gejyo, F., Yamada, T., Odani, S., Nakagawa, Y., Arakawa, M., Kunitomo, T., Kataoka, H., Suzuki, M., Hirasawa, Y., Shirahama, T., Cohen, A. S., and Schmid, K. (1985) *Biochem. Biophys. Res. Commun.* **129,** 701–706
4. Uchanska-Ziegler, B., and Ziegler, A. (2003) *Trends Immunol.* **24,** 73–76
5. Verdone, G., Corazza, A., Viglino, P., Pettirossi, F., Giorgetti, S., Mangione, P., Andreola, A., Stoppini, M., Bellotti, V., and Esposito, G. (2002) *Protein Sci.* **11,** 487–499
6. Esposito, G., Michelutti, R., Verdone, G., Viglino, P., Hernández, H., Robinson, C. V., Amoresano, A., Dal Piaz, F., Monti, M., Pucci, P., Mangione, P., Asti, L., Stoppini, M., Merlini, G., Ferri, G., and Bellotti V. (2000) *Protein Sci.* **9,** 831–845
7. Bellotti, V., Stoppini, M., Mangione, P., Sunde, M., Robinson, C. V., Asti, L., Brancaccio, D., and Ferri, G. (1998) *Eur. J. Biochem.* **258,** 61–67
8. McParland, V. J., Kalverda, A. P., Homans, S. W., and Radford, S. E. (2002) *Nat. Struct Biol.* **9,** 326–331
9. Hoshino, M., Katou, H., Hagihara, Y., Hasegawa, K., Naiki, H., and Goto, Y. (2002) *Nat. Struct. Biol.* **9,** 332–336
10. Trinh, C. H., Smith, D. P., Kalverda, A. P., Phillips, S. E., and Radford, S. E. (2002) *Proc. Natl. Acad. Sci. U. S. A.* **99,** 9771–9776
11. Tsunenaga, M., Goto, Y., Kawata, Y., and Hamaguchi, K. (1987) *Biochemistry* **26,** 6044–6051
12. Santoro, M. M., and Bolen, D. W. (1988) *Biochemistry* **27,** 8063–8068
13. Pace, C. N. (1986) *Methods Enzymol.* **131,** 266–280
14. Chiti, F., Mangione, P., Andreola, A., Giorgetti, S., Stefani, M., Dobson, C. M., Bellotti, V., and Taddei, N. (2001) *J. Mol. Biol.* **307,** 379–391
15. Chiti, F., De Lorenzi, E., Grossi, S., Mangione, P., Giorgetti, S., Caccialanza, G., Dobson, C. M., Merlini, G., Ramponi, G., and Bellotti, V. (2001) *J. Biol. Chem.* **276,** 46714–46721

16. Braunschweiler, L., and Ernst, R. R. (1983) *J. Magn. Reson.* **53,** 521–528
17. Piantini, U., Sørensen, O. W., and Ernst, R. R. (1982) *J. Am. Chem. Soc.* **104,** 6800–6801
18. Jeener, J., Meier, B. H., Bachmann, P., and Ernst, R. R. (1979) *J. Chem. Phys.* **71,** 286–292
19. Piotto, M., Saudek, V., and Sklenar, V. (1992) *J. Biomol. NMR* **2,** 661–665
20. Hwang, T. L., and Shaka, A. J. (1995) *J. Magn. Reson.* **112,** 275–279
21. Marion, D., and Wüthrich, K. (1983) *Biochem. Biophys. Res. Commun.* **113,** 967–974
22. States, D. J., Haberkorn, R. A., and Ruben, D. J. (1982) *J. Magn. Reson.* **48,** 286–292
23. Keeler, J., Clowes, R. T., Davis, A. L., and Laue, E. D. (1994) *Methods Enzymol.* **239,** 145–207
24. Bax, A., and Davis, D. G. (1985) *J. Magn. Reson.* **65,** 355–360
25. Shaka, A. J., Lee, C. J., and Pines, A. (1988) *J. Magn. Reson.* **77,** 274–293
26. Dayringer, H. E., Tramontano, A., Sprang, S. R., and Fletterick, R. J. (1986) *J. Mol. Graphics* **6,** 82–87
27. Koradi, R., Billeter, M., and Wüthrich, K. (1996) *J. Mol. Graphics* **14,** 51–55
28. Madura, J. D., Briggs, J. M., Wade, R. C., Davis, M. E., Luty, B. A., Ilin, A., Antosiewicz, J., Gilson, M. K., Bagheri, B., Scott, L. R., and McCammon, J. A. (1995) *Computer Phys. Commun.* **91,** 57–95
29. Antosiewicz, J., McCammon, J. A., and Gilson, M. K. (1994) *J. Mol. Biol.* **238,** 415–436
30. Fogolari, F., Ragona, L., Licciardi, S., Romagnoli, S., Michelutti, R., Ugolini, R., and Molinari, H. (2000) *Proteins* **39,** 317–330
31. Eisenberg, D., and McLachlan, A. D. (1986) *Nature* **319,** 199–203
32. Eakin, C. M., Knight, J. D., Morgan, C. J., Gelfand, M. A., Miranker, A. D. (2002) *Biochemistry* **41,** 10646–11065
33. Wüthrich, K. (1986) *NMR Spectroscopy of Proteins and Nucleic Acids*, Wiley & Sons, New York
34. Okon, M., Bray, P., and Vucelic, D. (1992) *Biochemistry* **31,** 8906–8915
35. Wishart, D. S., and Sykes, B. D. (1994) *Methods Enzymol.* **239,** 363–392
36. Naiki, H., Hashimoto, N., Suzuki, S., Kimura, H., Nakakuki, K., and Gejyo, F. (1997) *Amyloid Int. J. Exp. Clin. Invest.* **4,** 223–232
37. McParland, V. J., Kad, N. M., Kalverda, A. P., Brown, A., Kirwin-Jones, P., Hunter, M. G., Sunde, M., and Radford, S. E. (2000) *Biochemistry* **39,** 8735–8746
38. Morgan, C. J., Gelfand, M., Atreya, C., and Miranker, A. D. (2001) *J. Mol. Biol.* **309,** 339–345
39. Saper, M. A., Bjorkman, P. J., and Wiley, D. C. (1991) *J. Mol. Biol.* **219,** 277–319
40. Yang, A., and Honig, B. (1993) *J. Mol. Biol.* **231,** 459–474
41. Monti, M., Principe, S., Giorgetti, S., Mangione, P., Merlini, G., Clark, A., Bellotti, V., Amoresano, A., and Pucci, P. (2002) *Protein Sci.* **11,** 2362–2369
42. De Lorenzi, E., Grossi, S., Massolini, G., Giorgetti, S., Mangione, P., Andreola, A., Chiti, F., Bellotti, V., and Caccialanza, G. (2002) *Electrophoresis* **23,** 918–925
43. Rosano, C., Zuccotti, S., Mangione, P., Giorgetti, S., Bellotti, V., Pettirossi, F., Corazza, A., Viglino, P., Esposito, G., and Bolognesi, M. (2003) *J. Mol. Biol.* **335,** 1051–1064
44. Jones, S., Smith, D. P., and Radford, S. E. (2003) *J. Mol. Biol.* **330,** 935–941
45. Smith, D. P., Jones, S., Serpell, L. C., Sunde, M., and Radford, S. E. (2003) *J. Mol. Biol.* **330,** 943–954
46. Kozhukh, G. V., Hagihara, Y., Kawakami, T., Hasegawa, K., Naiki, H., and Goto, Y. (2002) *J. Biol. Chem.* **277,** 1310–1315
47. Katou, H., Kanno, T., Hoshino, M., Hagihara, Y., Tanaka, H., Kawai, T., Hasegawa, K., Naiki, H., and Goto, Y. (2002) *Protein Sci.* **11,** 2218–2229
48. Ohhashi Y., Hagihara, Y., Kozhukh, G. V., Hasegawa, K., Yamaguchi, I., Naiki, H., and Goto, Y. (2002) *J. Biochem.* (*Tokyo*) **131,** 45–52
49. Lomakin, A., Teplow, D. B., Kirschner, D. A., and Benedek, G. B. (1997) *Proc. Natl. Acad. Sci. U. S. A.* **94,** 7942–7947
50. Serio, T. R., Cashikar, A. G., Kowal A. S., Sawicki, G. J., Moslehi, J. J., Serpell, L., Arnsdorf, M F., and Lindquist, S. L. (2000) *Science* **289,** 1317–1321
51. Kelly, J. W. (2000) *Nat. Struct. Biol.* **7,** 824–826
52. Bitan, G., Kirkitadze, M. D., Lomakin, A., Vollers, S. S., Benedek, G. B., and Teplow, D. B. (2003) *Proc. Natl. Acad. Sci. U. S. A.* **100,** 330–335
53. Zhang, S., Iwata, K., Lachenmann, M. J., Peng J. W., Li, S., Stimson, E. R., Lu, Y.-a, Felix, A. M., Maggio, J. E., and Lee, J. P. (2000) *J. Struct. Biol.* **130,** 130–141
54. Kayed, R., Head, E., Thompson, J. L., McIntire, T. M., Milton, S. C., Cotman, C. W., and Glabe, C. G. (2003) *Science* **300,** 486–489